scientific reports

OPEN

# Effect of electrode size and distance to tissue on unipolar and bipolar voltage electrograms and their implications for a near-field cutoff

Vincent Schlageter[1,2], Adrian Luca[3], Patrick Badertscher[1,2], Philipp Krisai[1,2], Thomas Kueffer[4], David Spreen[1,2], Josip Katic[2], Stefan Osswald[1,2], Beat Schaer[1,2], Christian Sticherling[1,2], Michael Kühne[1,2] & Sven Knecht[1,2]✉

**Characteristics of electrograms depend on the electrode design and distance to the electric source. Our aim was to assess the impact of electrode design and distance from the myocardial electric source on the unipolar and bipolar electrograms to deduce a far-field cut-off. We retrospectively analyzed left atrial electroanatomical maps of 25 patients acquired using an ablation catheter with a 4.5 mm tip-, mini- and 2 mm ring electrodes. The unipolar and bipolar electrograms were characterized based on peak-to-peak amplitude, signal duration, maximal slope, and relative power of the high frequency spectrum above 50 Hz (HF_rel). The unipolar electrograms of ring electrodes showed an increased amplitude (140%), slope (150%) and HF_rel (16% vs. 11%) compared to the tip- and mini-electrodes. The median amplitude, slope, and HF_rel for the ring electrodes followed a power-law decay with distance with a steep decline up to 4 mm. This near-field cut-off can be identified based on a HF_rel above 10% in unipolar electrograms. In conclusion, we observed a higher unipolar amplitude for small ring-electrodes compared to larger tip-electrodes. The rapid decay of the amplitude, slope, and HF_rel up to a distance of 4 mm is suggestive for near-field cut-off identified based on HF_rel above 50 Hz.**

**Clinical Trial Registration: NCT04095559.**

**Keywords** Unipolar, Bipolar, Electrogram, Electrode, Distance, Near-field

**Abbreviations**

| | |
|---|---|
| BV | Bipolar voltage |
| EGM | Electrogram |
| HF_rel | Relative power of the high-frequency spectrum above 50 Hz |
| LAVI | Indexed left atrial volume |
| LVEF | Left ventricular ejection fraction |
| LA | Left atrium |
| UV | Unipolar voltage |

The characteristics of unipolar and bipolar voltage electrograms (EGM) acquired by electrophysiological catheters depend on the electrical source as well as on the sensing electrode configuration. The resulting EGM is used to identify the timing of the electrical activation and to characterize the myocardial substrate to perform catheter ablation. Despite following this basic principle for decades, the exact relationship between electrical source and resulting unipolar voltage (UV) and bipolar voltage (BV) EGM is still not completely understood. The UV EGM reflects the far-field and near-field information of the cellular depolarization wavefront traveling

[1]Department of Cardiology, University Hospital Basel, University of Basel, Petersgraben 4, Basel 4031, Switzerland. [2]Cardiovascular Research Institute Basel, University Hospital Basel, University of Basel, Basel, Switzerland. [3]Department of Cardiology, Lausanne University Hospital and University of Lausanne, Lausanne, Switzerland. [4]Department of Cardiology, Inselspital, Bern University Hospital, University of Bern, Bern, Switzerland. ✉email: sven.knecht@usb.ch

along the electrode. The BV EGM, however, calculated as the difference between two unipolar electrodes, eliminates a large fraction of the far-field information and mainly reflects the local near-field information[1,2]. However, the BV EGM strongly depends on the electrode pair orientation relative to the electrical activation wavefront. This limitation was recently addressed to some extent by the introduction of multipolar diagnostic catheters and dedicated software allowing to calculate an orientation-independent BV EGM[3–6]. The impact of the distance between the electrical source and the electrodes on the EGM characteristics (electrode-tissue distance) in general, however, is still not known. This is of high clinical relevance to reliably characterize the underlying substrate and to be able to successfully plan and perform safe and effective catheter ablation procedures. For the latter, it is crucial to know whether the electrical signals are within the reach of the ablation energy. Finally, despite being used in daily clinical practice, the cut-off to differentiate between far-field and near-field EGM has never been quantitatively specified.

Hence, the aim of this study was to assess the impact of the electrode type and electrode-tissue distance from the electric source on the bipolar and unipolar intracardiac EGM recorded with a multi-electrode ablation catheter and to deduce a potential cut-off for far-field versus near-field discrimination.

## Methods

We analyzed the left atrial (LA) 3D electroanantomical maps (EAMs) from the prospective CHAZE study (ClinicalTrials.gov Identifier: NCT04095559). In this study, 25 patients with atrial fibrillation underwent detailed mapping of the LA in sinus rhythms prior to repeat catheter ablation. This allowed us to cover a wide range of tissue characteristics from healthy to fibrotic tissue. The study was approved by the local ethics committee (Ethics Committee Northwest and Central Switzerland) and was conducted in accordance with the Declaration of Helsinki.

### Electrogram acquisition

The LA EAM was acquired in sinus rhythm using the IntellaNav Mifi OI catheter as previously described using the Rhythmia system (Boston Scientific, USA)[7]. In brief, the LA anatomy was mapped using the IntellaNav Mifi OI catheter (7.5 Fr, 4.5 mm tip electrode size, mini electrode size 0.5 $mm^2$ with 2.4 mm interelectrode spacing and 1.3 mm from tip; 2 mm ring electrode with 2.5 mm interelectrode spacing) and projected onto the previously mapped EAM shell using the Orion catheter when within 3 mm of it. Electrode surfaces of the tip-, ring- and mini-electrode measure 30 $mm^2$, 10 $mm^2$ and 0.5 $mm^2$, respectively. The bipolar voltage (BV) and unipolar voltage (UV) were filtered at 10–250 Hz with a sampling rate of 1 kHz.

### Electrogram analysis

The exported study data included the location and BV and UV EGMs of all three electrode types (tip-, ring-, and mini-electrode) and the anatomical shell. The data was processed and analyzed in Matlab (MATLAB (2021) Natick, Massachusetts, USA) as follows: The effective electrode-tissue distance between tissue and electrode was calculated based on the position of the electrode and its projection to the surface shell of the EAM. For analysis, the values were categorized into four prespecified groups based on the catheter orientation as parallel (0°–14°), medium low (15°–34°), medium high (35°–59°), and perpendicular (60°–90°) orientation (Fig. 1). Angles between 90° and 180° were considered mirror images and included accordingly in these groups. The influence of the electrode dimension on the EGM characteristics was deduced from the parallel orientation group, whereas the two medium and the perpendicular orientation groups were used to deduce the electrode-tissue distance dependency of the ring electrodes.

The EGMs were quantified based on the peak-to-peak amplitude (amp), the duration between min and max value (width), the maximal slope dV/dt between the minimal and maximal values, and the relative power of the high-frequency spectrum above 50 Hz (HF_rel). The latter was calculated using fast Fourier transform (FFT) as recently published[8]. Briefly, the power of the high-frequency spectrum was calculated for a frequency cut-off of 50 Hz (50–300 Hz) and normalized by the power spectrum of the entire spectrum. Except for the HF_rel, for which absolute values are reported, all feature values are normalized by dividing them by the values from the tip-electrode (for unipolar) or the tip-to-ring pairs (for bipolar measures) as a reference with confirmed closest electrode-tissue distance.

### Statistical analysis

Continuous variables are expressed as median with Interquartile range (IQR). To investigate the relationship between the above-described features and the electrode-tissue distance, we plotted all features over the distance between the electrode center-of-mass and the myocardial surface. Given the inverse relationship between the electric field strength and distance from the source, we performed a power regression analysis (Microsoft Excel 365, Microsoft Corporation) to best describe this relationship.

## Results

We analyzed EGMs of 5180 catheter locations based on the four features amplitude, width, slope, and HF_rel from 25 patients (72% male, age 68 ± 15 years, LVEF 59 ± 8%, LA size 41 ± 8 mm, LAVI 38 ± 9 ml/$m^2$). Thereof, 1345 EGMs were from parallel, 1826 from medium low, 1588 from medium high, and 421 EGMs from perpendicular catheter orientation. The median value of the UV amplitude at the tip and BV tip-ring amplitude for all points was 1.01 mV (IQR: 0.41mV, 1.55 mV) and 0.79 mV (IQR: 0.41 mV, 1.55 mV), respectively. The slopes for the UV and BV were 0.10 mV/ms (IQR: 0.06 mV/ms, 0.19 mV/ms) and 0.09 mV/ms (IQR: 0.06 mV/ms, 0.18 mV/ms) and for the width 16 ms (IQR: 10 ms, 29 ms ) and 10 ms (IQR: 7 ms, 16 ms), respectively.

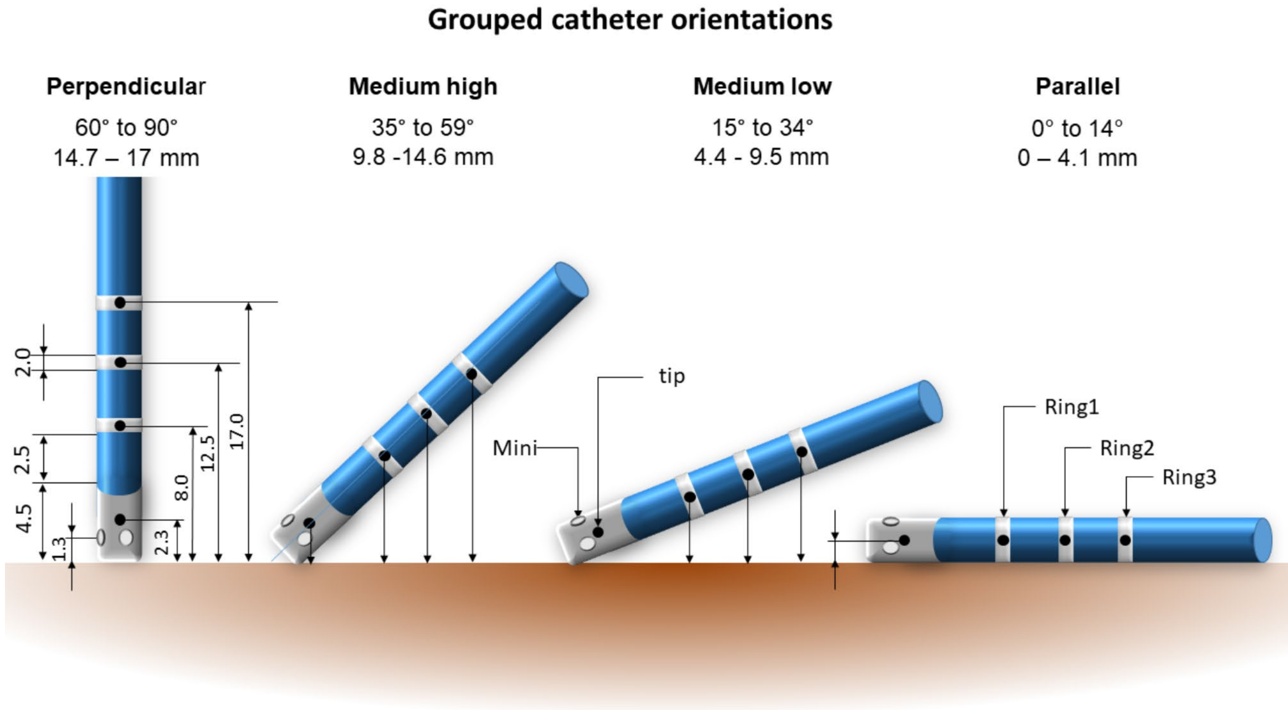


**Fig. 1**. Catheter orientation, dimension, and electrode-tissue distance (min and max distance in mm for the ring3 electrode). The perpendicular and tilted catheter orientations were used to investigate the impact of electrode type and distance on the EGM. In contrast, the parallel catheter orientation was used to investigate the impact of electrode configuration only due to the comparable electrode-tissue distance. The black dots represent the center-of-mass of the electrodes for which the distances were reported based on the projection to the tissue.

| Configuration | | Dist [mm] | Amp [%] | Width [%] | Slope [%] | HF_rel [%] |
|---|---|---|---|---|---|---|
| Unipolar | tip | 1.25 | 100 | 100 | 100 | 11 |
| | ring1 | 2.13 | 142 | 91 | 166 | 15 |
| | ring2 | 2.51 | 141 | 88 | 183 | 16 |
| | ring3 | 3.14 | 120 | 91 | 140 | 17 |
| | M1 | 1.30 | 98 | 100 | 100 | 16 |
| | M2 | 1.30 | 107 | 98 | 110 | 14 |
| | M3 | 1.30 | 104 | 100 | 108 | 14 |
| Bipolar | tip-ring1 | 1.69 | 100 | 100 | 100 | 39 |
| | ring1-ring2 | 2.32 | 83 | 96 | 88 | 51 |
| | ring2-ring3 | 2.82 | 63 | 110 | 63 | 46 |
| | M1-M2 | 1.30 | 60 | 89 | 61 | 52 |
| | M2-M3 | 1.30 | 54 | 95 | 57 | 50 |
| | M3-M1 | 1.30 | 58 | 94 | 61 | 43 |

**Table 1**. Parameters for the uni- and bipolar EGMs for the three electrode types for the parallel orientation. Values of amp, width and slope are normalized using the tip-electrode for unipolar and the tip-to-ring pairs for bipolar signals. Amp, voltage amplitude; Dist, distance from tissue; M, mini-electrode.

### Impact of electrode size on the EGM characteristics

Based on the analysis of the parallel catheter orientation with all electrodes being in close proximity to the tissue, the three smaller ring electrodes showed an increased UV amplitude (mean: 134%) and increased slope (mean: 163%) compared to the tip electrode. Their mean HF_rel was increased by absolute 5% compared to the larger tip (Table 1). Furthermore, the signal width was smaller for the ring compared to the tip electrode. For the mini-electrodes, amplitude, slope, and width are similar to the larger tip electrode. In the parallel orientation, however, with one electrode being potentially in full contact with the tissue whereas the other electrodes are at 2.5 mm distance based on the catheter diameter, a larger variation was observed in the amplitude and slope of 8–10%. Based on the analysis of the perpendicular catheter orientation with the mini-electrodes being all in comparable distance from the tissue within around 1.3 mm, their variation in the unipolar EGM features was relatively small (absolute difference of 2%) (Supplemental Fig. 1).

For the bipolar EGMs, the tip- ring pair showed the largest amplitude, width, and slope. The HF_rel component was larger for all electrode pairs compared to the corresponding unipolar EGM, but lowest for the tip-ring1 electrode pair.

Of note, the ring electrodes showed a strong dependency on the catheter orientation in all features, whereas the values of the tip electrodes with a stable contact to the tissue remained comparable (Supplemental Fig. 1).

### Relationship between ECG features and electrode-tissue distance

The electrode specific relationship between the electrode-tissue distance and the EGM features are shown in Fig. 2 for unipolar and Fig. 3 for bipolar EGMs. The three features amp, slope, and HF_rel followed a power-law decay function ($R^2 = 0.97$, $R^2 = 0.95$ and $R^2 = 0.79$, respectively), whereas the EGM width increases linearly with electrode-tissue distance from the tissue ($R^2 = 0.96$). Since the catheter tip was required to be in contact with the tissue during mapping, the information on distance-dependency of the tip and mini-electrode is limited. Of note, the decline for the three features is less pronounced for the bipolar amplitude compared to the unipolar amplitude, representing the local characteristics of the bipolar EGM.

The gradients of the fitted curves for the two features amp and slope gradually decrease between 4 mm and 6 mm distance, as reflected by the angulation of the two linear approximations (dash-dotted line, Figs. 2 and 3) for close and distant points at their intersection (red circles, Figs. 2 and 3). Accordingly, this distance up to 4 mm was defined as near-field, which could be confirmed for the bipolar EGMs. At this cut-off, a HF_rel value of > 10% for unipolar (Fig. 2, red arrow) and > 30% for bipolar EGMs (Fig. 3, red arrow) would allow to identify all near-field ring-electrode signals.

## Discussion

Unipolar and bipolar EGMs are mostly characterized qualitatively based on their visual appearance as near-field or distant far-field EGM source. Except for numerical simulations, the relationship of EGM characteristics and electrode-tissue distance to deduce a distance-EGM relationship has not been characterized quantitatively. In our detailed analysis of EAMs of the LA, we could observe the following: (1) The ring electrodes with a smaller surface area than the tip showed a larger amplitude, slope, and high frequency component HF_rel and a narrower signal width. For bipolar EGM, however, the ring electrode pairs showed a lower amplitude, slope, and HF_rel compared to the distal tip-ring electrode. (2) The mini-electrodes showed unipolar features comparable to the tip electrode. However, based on the higher variation of the unipolar signals in parallel compared to

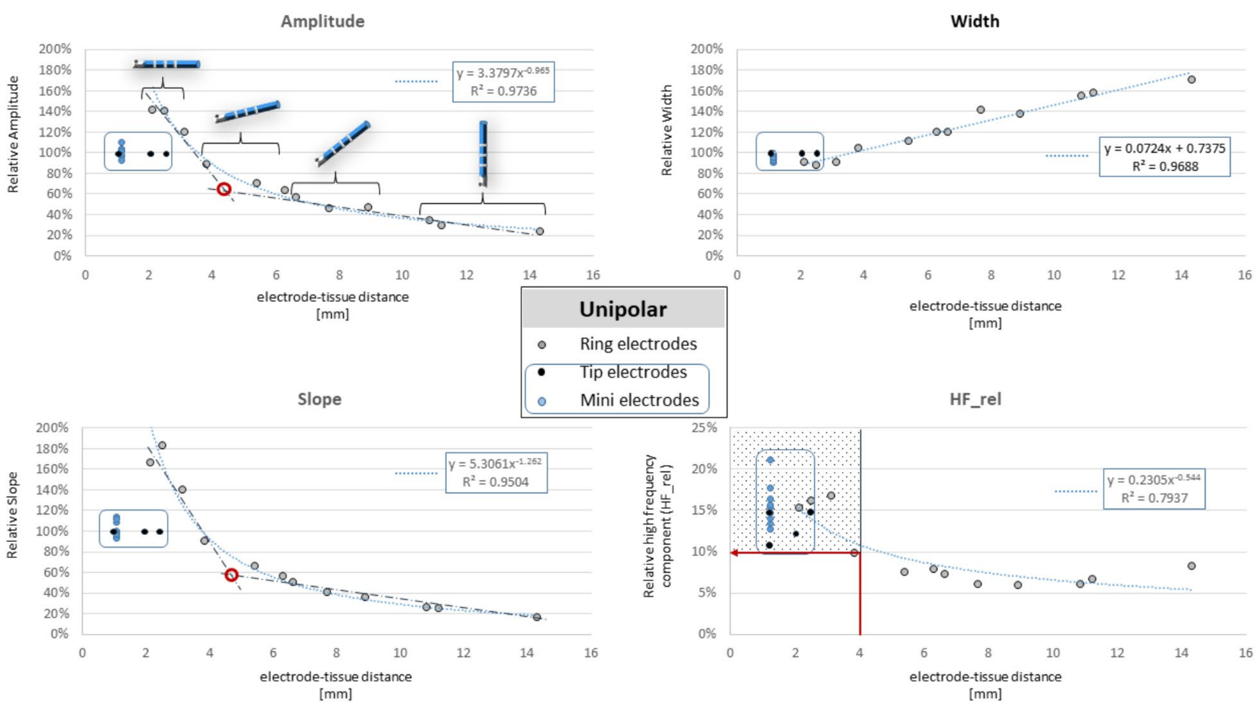


**Fig. 2**. Feature-distance plot of the unipolar EGM for the amplitude, width, slope, and relative power of the high-frequency spectrum (HF_rel). The grey dots of the ring electrodes represent the mean values of the three electrodes in the four groups. The blue dotted line reflects the best fit. The blue line encloses the features obtained from the catheter tip (tip-, and mini-electrodes).

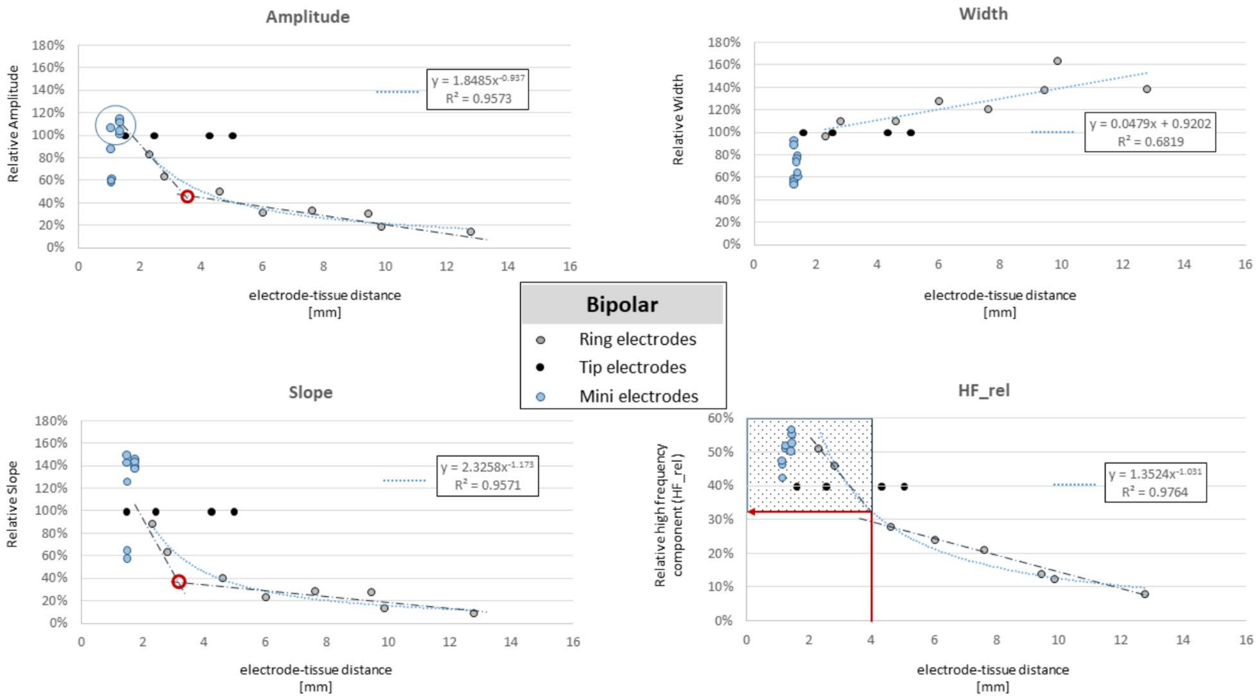


**Fig. 3**. Feature-distance plot of the bipolar EGM for the amplitude, width, slope, and relative power of the high-frequency spectrum (HF_rel). The grey dots of the ring electrodes represent the mean values of the three electrodes in the four groups. The blue dotted line reflects the best fit.

perpendicular orientation, a strong relationship with distance might be characteristic for this electrode type. (3) The amplitude, slope, and HF_rel for the ring electrodes showed all a strong power-law decay function with electrode-tissue distance, whereas the EGM width increases linearly with distance from the tissue. This could be observed for the unipolar and for the bipolar EGMs. (4) A steep linear decline for a distance up to 4 mm is suggestive for a strong near-field relationship, whereas the flat decay above 6 mm is suggestive of mainly far-field impact. Based on this value of 4 mm, a near-field cut-off for the unipolar and bipolar electrogram with a HF_rel of 10% and 30%, respectively, appears reasonable.

## Impact of electrode size

It is commonly considered that the smaller the electrode is, the larger the amplitude of the unipolar EGM should be. We could confirm this assumption in our study for the ring electrodes but not for the mini electrodes, which showed similar UV amplitude to the tip electrode. This might be explained at least in parts by the spatial distribution of the mini electrode on the tip of the catheter and is in line with the results using another microelectrode catheter (Qdot, Biosense Webster)[9]. Whereas one electrode is in direct tissue contact in the parallel catheter orientation, the other mini electrode might be more than 2 mm away from the tissue. Due to the missing information of the exact mini-electrode position in the 3D EAM data, however, we could report the UV features for all electrodes for the same approximated location of 1.3 mm only. Further in vivo comparisons to investigate the impact of electrode size on the EGM are rare. The comparison of another micro-electrode ablation catheter (Qdot, Biosense Webster, USA) with a multipolar diagnostic catheter (Pentaray, Biosense Webster, USA) in porcine infarction models revealed a moderate linear relationship between the BV EGMs of the two catheters[10]. Whereas in healthy ventricular tissue, the smaller micro-electrodes showed larger bipolar electrograms compared to the ring-electrodes from the Pentaray or the tip electrode of the ablation catheter, this difference diminished in diseased, fibrotic tissue. In our preceding study comparing the bipolar EGM in repeat procedure after index PVI, we even identified lower BV amplitude for the catheters with smaller electrode surface, such as the Orion or the circular Lasso catheter compared to the larger tip electrode[7]. A reason might be the interplay between interelectrode spacing in BV EGMs, spatial fibrosis distribution and amplitude of the electrical source, as well as wavefront propagation direction. In another study using UV EGMs from a multipolar catheter (Octaray, Biosense Webster, USA), the area of interest with scar tissue could be better delineated than using the bipolar electrogram[11]. However, a two-layer viable myocardium (with midmyocardial scar) could be identified more reliable using the BV EGM.

## Frequency based analysis

In most studies the EGM classification based on local, high-frequency, multicomponent signals was performed qualitatively based on the physicians judgement[12–14]. Recently, however, frequency-based analysis to characterize and classify the LV substrate were published[15,16]. Instead of manual annotation of local abnormal ventricular activity, late potentials (LP), or deceleration zone (DZ), this area of fractionation could be identified with a sensitivity of 91% and specificity of 85% by applying a 220 Hz frequency cut-off value in areas of low bipolar voltage based on the HD grid bipolar voltage map[15]. The smaller ring-electrodes with a length of 1 mm and diameter of 0.8 mm might explain the higher frequency cutoff compared to our applied 50 Hz value. Furthermore, our aim was to discriminate near-field from far-field signal and not to identify areas with abnormal local EGM in low voltage areas based on a machine learning algorithm. Prediction of midmyocardial fibrosis from late-iodine computed tomography scans based of detailed frequency-based EGM analysis was performed in 13 patients with non-ischemic cardiomyopathy using a 3.5 mm tip ablation catheter[16]. They reported that frequency-feature based classifiers better predict the presence of midmyocardial fibrosis. In conclusion, both studies confirm the potential of frequency feature extraction from intracardiac EGM to gain a deeper insight into and understanding of the origin of the sensed unipolar and bipolar EGM.

### Impact of electrode-tissue distance from tissue

Over a distance up to 14 mm from the tissue, we observed a power-law decay for the voltage, slope, and the fraction of high frequency components HF_rel. The decay function property is in line with the results from a surgical study in patients with paroxysmal and persistent AF[17]. Based on the experimental data of 10 s unipolar EGMs from a high-density electrode array and a computer simulation, they observed a decay to 50% of the source unipolar EGM within 1.5–2.1 mm function. This is in the same range for the ring electrode in our study between 2 and 4 mm distance (140–70% for amplitude and 180–90% for the slope).

Of note, within the close electrode-tissue distance of 4 mm of the ring electrodes from the tissue, we observed a linear decline of the amplitude and slope of the unipolar and bipolar EGMs, whereas the signal width remains constant. Furthermore, within this boundary, the fraction of high-frequency components above 50% (HF_rel) in the overall EGM is higher than at more distant positions. This observation reinforces the usage of these features for far-field discrimination. Furthermore, the 4 mm electrode-tissue distance is in the range of a radiofrequency lesions size and consequently clinically relevant[18].

### Implications for clinical far-field and near-field discrimination

Despite being mentioned and used in numerous studies on signal analysis and interpretation, the term near-field and far-field is not yet quantified in the field of EP. Currently, the EGMs are mainly classified based on the qualitative signal characteristics, such as fractionation, sharpness, or high frequency EGMs[12,13]. Whereas fractionation can be quantified and reproduced, a signal "sharpness" or presence of "high-frequency" components are still undefined.

To classify the EGM into near-field and far-field based on a specified boundary depends on one hand on the technical background (e.g. source and electrode characteristics) but as well on the ability to reach and eliminate the target EGM by ablation. With recent ablation technologies, lesion depth around 4–5 mm can be created[19,20]. Based on this procedural criterion, the deduced cut-off at 4 mm might be comprehensible. This electrode-tissue distance might be represented for all electrode types in the healthy tissue above 0.5 mV by a relative HF component with a 50 Hz above 10% and 30% based on the unipolar and bipolar EGM, respectively. To verify these values, however, further prospective studies investigating the application as well on smaller tip electrode sizes of commonly 3.5 mm are recommended.

### Limitations

First, the acquired 3D-EAM might not reflect the actual location of the myocardium acting as the relevant electric source, potentially undermining the calculated electrode-tissue distances. Second, the observed relationship and deduced cut-off are only valid for atrial tissue. Especially for the ventricle with thicker myocardial tissue and consequently larger voltage values and differences in frequency composition, difference in values must be expected and needs to be elaborated. Fourth, in parallel orientation, the catheter might cover not purely the same tissue with the same electrical source and characteristics. As consequence, the observed difference between tip and ring electrodes might arise as well from differences of the source characteristics and not purely of the electrodes. Fifth, in contrast to an electrode in contact with the tissue, our electrodes are surrounded by the blood pool in with a different conductivity than the tissue, which might have an impact on the sensed EGM characteristic. Sixth, we could not investigate the influence of catheter distance for the tip electrode since all mapped points were with the tip in contact with the tissue. Seventh, even though the physicians acquiring the EAM are all very experienced and assessed the tip-to-tissue contact based on the catheter movement, tactile feedback, signal and signal characteristics, definite tissue contact cannot be guaranteed. Based on the calculation of mean values over hundreds of measurements for the four groups, this potential impact on our results is reduced Finally, whether the cutoffs deduced from the ring electrodes are transferable to the tip electrode with different size needs further investigation.

## Conclusion

A strong relationship of the unipolar and bipolar EGMs with electrode size and electrode-tissue distance could be observed. We observed a higher unipolar amplitude for small ring-electrodes compared to larger tip-electrodes. Furthermore, a decay of the amplitude, slope, and HF_rel with distance could be observed. This decay functions are suggestive for a near-field cut-off distance below 4 mm from the tissue, which is reflected by a high HF_rel of 10% and 30% for the unipolar and bipolar EGM, respectively. Further studies are warranted to confirm this observation.

## Data availability
The data that support the findings of this study are available from the corresponding author, [SK], upon reasonable request.

Received: 7 August 2024; Accepted: 4 November 2024
Published online: 08 November 2024

## References
1. Tedrow, U. B. & Stevenson, W. G. Recording and interpreting unipolar electrograms to guide catheter ablation. *Heart Rhythm* **8**, 791–796 (2011).
2. de Groot, N. M. S. et al. Critical appraisal of technologies to assess electrical activity during atrial fibrillation: a position paper from the European Heart Rhythm Association and European Society of Cardiology Working Group on eCardiology in collaboration with the Heart Rhythm Society, Asia Pacific Heart Rhythm Society, Latin American Heart Rhythm Society and Computing in Cardiology. *EP Europace* **24**, 313–330 (2022).
3. Dittrich, S. et al. The omnipolar mapping technology—a new mapping tool to overcome bipolar blindness resulting in true high-density maps. *J. Interv Card Electrophysiol.* https://doi.org/10.1007/s10840-023-01562-4 (2023).
4. Takigawa, M. et al. Detailed analysis of the relation between bipolar electrode spacing and far- and near-field electrograms. *JACC: Clin. Electrophysiol.* **5**, 66–77 (2019).
5. Padilla, J. R. et al. Orientation of conduction velocity vectors on cardiac mapping surfaces. *EP Europace* **25**, 1172–1182 (2023).
6. Porta-Sánchez, A. et al. Omnipolarity applied to equi-spaced electrode array for ventricular tachycardia substrate mapping. *EP Europace* **21**, 813–821 (2019).
7. Knecht, S. et al. Atrial substrate characterization based on bipolar voltage electrograms acquired with multipolar, focal and mini-electrode catheters. *EP Europace* **25**, 1–8 (2023).
8. Schlageter, V. et al. A single-beat algorithm to discriminate farfield from nearfield bipolar voltage electrograms from the pulmonary veins. *J. Interv Card Electrophysiol.* **66**, 2047–2054 (2023).
9. Omara, S. et al. Multisize electrode field-of-view: validation by high resolution gadolinium-enhanced cardiac magnetic resonance. *JACC: Clin. Electrophysiol.* **10**, 637–650 (2024).
10. Glashan, C. A. et al. Mini-, micro-, and conventional electrodes: an in vivo electrophysiology and ex vivo histology head-to-head comparison. *JACC Clin. Electrophysiol.* **7**, 197–205 (2021).
11. Glashan, C. A. et al. Multielectrode unipolar voltage mapping and electrogram morphology to identify post-infarct scar geometry. *JACC: Clin. Electrophysiol.* **8**, 437–449 (2022).
12. Jaïs, P. et al. Elimination of local abnormal ventricular activities. *Circulation* **125**, 2184–2196 (2012).
13. de, R. M. et al. Targeting the hidden substrate unmasked by right ventricular Extrastimulation improves ventricular tachycardia ablation outcome after myocardial infarction. *JACC: Clin. Electrophysiol.* **4**, 316–327 (2018).
14. Ye, Z. et al. Characterization of unipolar electrogram morphology: a novel tool for quantifying conduction inhomogeneity. *EP Europace* **25**, euad324 (2023).
15. Payne, J. E. et al. A novel automated peak frequency annotation algorithm for identifying deceleration zones and ventricular tachycardia ablation sites. *Heart Rhythm* **S1547-5271**(23), 02805–02809. https://doi.org/10.1016/j.hrthm.2023.10.014 (2023).
16. Whitaker, J. et al. Frequency domain analysis of endocardial electrograms for detection of nontransmural myocardial fibrosis in nonischemic cardiomyopathy. *JACC: Clin. Electrophysiol.* **9**, 923–935 (2023).
17. Podziemski, P. et al. Far-field effect in unipolar electrograms revisited: High-density mapping of atrial fibrillation in humans. In *37th Annual International Conference of the IEEE Engineering in Medicine and Biology Society (EMBC)* 5680–5683. https://doi.org/10.1109/EMBC.2015.7319681 (2015).
18. Ikenouchi, T. et al. Comparison of lesion characteristics using temperature-flow-controlled versus conventional power-controlled ablation with fixed ablation index. *J. Cardiovasc. Electrophys.* **34**, 908–917 (2023).
19. Yamaguchi, J. et al. Comparison of three different approaches to very high-power short-duration ablation using the QDOT-MICRO catheter. *J. Cardiovasc. Electrophysiol.* **34**, 888–897 (2023).
20. Nakagawa, H. et al. Effects of contact force on Lesion size during pulsed field catheter ablation: histochemical characterization of ventricular lesion boundaries. *Circ. Arrhythm. Electrophysiol.* **2020**, e012026 (2020).

## Acknowledgements
None.

## Author contributions
Conceptualization: VS, SKExperiments & Data Acquisition: PB, PK, DS, JK, CS, MK, SKMethodology: VS, AL, PB, MK, SKWriting Draft Preparation: VS, SKReview and Editing: VS, AL, PB, PK, TK, DS, JK, SO, BS, CS, MK; SKFunding: SK, CS, SOProject Administration: VS, SK.

## Funding
The study was supported by an investigator sponsored grant (Boston Scientific, ISRRM10392).

## Competing interests
S Knecht has received funding from the Swiss Heart Foundation P Badertscher has received research funding from the University of Basel, the Stiftung für Herzschrittmacher und Elektrophysiologie, the Freiwillige Akademische Gesellschaft Basel, the Swiss Heart Foundation, and Johnson&Johnson and reports personal fees from BMS, Boston Scientific, and Abbott (all outside the submitted work). P Krisai reports speaker fees from BMSGrants, from the Swiss National Science Foundation, Swiss Heart Foundation, Foundation for Cardiovascular Research Basel, Machaon Foundation.C Sticherling is a member of Medtronic Advisory Board Europe and Boston Scientific Advisory Board Europe and has received educational grants from Biosense Webster and Biotronik, a research grant from the European Union's 7th Framework Programme and Biosense Webster, and lecture and consulting fees from Abbott, Medtronic, Biosense Webster, Boston Scientific, MicroPort, and Biotronik (all outside the submitted work). M Kühne reports grants from the Swiss National Science Foundation (grant numbers 33CS30_148474, 33CS30_177520, 32473B_176178, and 32003B_197524), the Swiss Heart Foundation, the Foundation for Cardiovascular Research Basel, the University of Basel, Bayer,

Pfizer, Boston Scientific, Bristol-Myers Squibb, and Biotronik and grants and personal fees from Daiichi Sankyo (all outside the submitted work). Others have nothing to declare.

## Ethics approval

The study was approved by the local ethics committee (Ethics Committee Northwest and Central Switzerland) and was conducted in accordance with the Declaration of Helsinki.

## Patient consent

Written informed consent was provided by all patients prior to the procedure.

## Additional information

**Supplementary Information** The online version contains supplementary material available at https://doi.org/10.1038/s41598-024-78627-5.

**Correspondence** and requests for materials should be addressed to S.K.

**Reprints and permissions information** is available at www.nature.com/reprints.

**Publisher's note** Springer Nature remains neutral with regard to jurisdictional claims in published maps and institutional affiliations.